Short Communication:

Codoping of Nickel and Nitrogen in ZrO_2-TiO_2 Composite as Photocatalyst for Methylene Blue Degradation under Visible Light Irradiation

Akhmad Syoufian[1*] and Rian Kurniawan[2]

[1]*Department of Chemistry, Faculty of Mathematics and Natural Sciences, Universitas Gadjah Mada, Sekip Utara, Yogyakarta 55281, Indonesia*

[2]*Institute of Chemical Technology, Universität Leipzig, Linnéstr. 3, Leipzig 04103, Germany*

** **Corresponding author:***

email: akhmadsyoufian@ugm.ac.id

Received: October 26, 2023
Accepted: April 9, 2024

DOI: 10.22146/ijc.90151

Abstract: *Nickel (Ni) and nitrogen (N) as codopants had been introduced into ZrO_2-TiO_2 composite photocatalyst. The objectives of this study are to investigate the codoping effect of Ni and N, as well as the calcination temperature towards the ability to photodegrade methylene blue (MB) under the irradiation of visible light. Different amounts of Ni dopant (w_{Ni}/w_{Ti} = 2–10%) along with a fixed amount of N dopant (w_N/w_{Ti} = 10%) were applied to the ZrO_2-TiO_2 composite through the sol-gel method. Crystallization of the composite was done by calcination at 500, 700, and 900 °C. Characterization of the composite was done using Fourier-transform infrared spectrophotometer (FTIR), X-ray diffractometer (XRD), specular reflectance UV-visible spectrophotometer (SR-UV) and scanning electron microscopy equipped with energy dispersive X-ray spectrometer (SEM-EDX). The photocatalytic activity of the composite was evaluated by photodegradation of 4 mg L^{-1} MB solution under visible light irradiation at various reaction times. The lowest band gap was achieved until 2.79 eV by the composite with 6% Ni and 10% N calcined at 900 °C. The highest MB degradation percentage up to 61% was obtained by the composite with 6% Ni and 10% N calcined at 500 °C (k_{obs} = 7.8 × 10^{-3} min^{-1}).*

Keywords: *methylene blue; codoping; photodegradation; ZrO_2-TiO_2*

■ INTRODUCTION

Methylene blue (MB) is a basic dye broadly applied in the textile industry and can pollute the environment, particularly the aquatic environment. Because MB is toxic, mutagenic, carcinogenic, and cannot be decomposed organically, it has a threshold value in water of 0.2 mg L^{-1} [1]. Various methods have been developed and implemented to remediate the dye-polluted water, such as adsorption [2-3], ion exchange [4], coagulation [5], reverse osmosis [6], enzyme [7] and electrochemical approach [8]. Most of those methods are costly and energy-demanding [9]. Photodegradation is an efficient, low-cost, and simple method for dealing with environmental dye waste pollution. Photodegradation requires photons as energy and catalysts to accelerate the degradation reaction. In treating water pollution caused by MB dye, photodegradation with a photocatalyst is the best option [10]. Photocatalysts are important in photodegradation because they can generate •OH radicals from water that decompose contaminants to CO_2 and H_2O [11].

Zirconium oxide, also known as zirconia (ZrO_2), is a material with photocatalytic potential due to several advantages. ZrO_2 exhibits low thermal conductivity, high mechanical properties and photo-thermal stability [12]. ZrO_2 also exhibits a band gap of ~5 eV, allowing it to produce a redox effect when exposed to ultraviolet (UV) radiation [13]. On the other hand, titanium dioxide (TiO_2) has been widely used as a photocatalyst because of its superior photocatalytic activity, chemical stability, redox potential, resistance to photo-corrosion,

non-toxicity, and low cost [14]. TiO_2 has a photocatalytic activity with band gaps of 3.0 and 3.2 eV for rutile and anatase phases, respectively, requiring only UV light to function [15]. Although the anatase possesses a wider band gap than rutile, it demonstrates better photoactivity under UV light irradiation compared rutile phase [16]. Owing to TiO_2 photocatalytic properties and ZrO_2 mechanical properties, coupling both semiconductors will benefit from larger surface area, higher thermal stability, and heat resistance [17]. Moreover, coupling ZrO_2-TiO_2 forms heterojunction and retards the recombination rate of photogenerated charges, thus improving photocatalytic efficiency [18].

Large ZrO_2-TiO_2 band gap (~3.2 eV) limits the photocatalytic activity in the range of UV irradiation [19]. One method for lowering the band gap of ZrO_2-TiO_2 is by introducing dopants. Takahashi et al. [20] found that using nickel as a doping agent reduced the band gap energy of TiO_2. Non-metal dopants work to capture holes, while metal dopants work to capture electrons. Sun et al. [21] discovered that using metal and non-metal dopants can increase hydrogen production by up to tenfold. The addition of nitrogen as a dopant can increase the conductivity of metal oxide ions [22]. N-doped TiO_2 exhibits 30% efficiency in degrading MB for 300 min under visible light irradiation [23]. Despite the poor activity in the visible region, the nitrogen role as dopant in TiO_2 can be improved by introducing a metal as a codopant [24]. On the other hand, Ni-doped TiO_2 is able to degrade 24 and 48% of MB for 120 min under the presence of UV and visible light, respectively [25]. Our previous studies [26-27] found that using iron (Fe) and copper (Cu) as metal codopant with nitrogen dopant in ZrO_2-TiO_2 composite demonstrates higher photocatalytic activity in degrading organic dye pollutants than undoped and N-doped ZrO_2-TiO_2 composite under visible light irradiation. Alternatively, codoping N and nickel (Ni) into TiO_2 also increases the photoactivity and suppresses the recombination of photogenerated electron-hole pairs, thus improving photocatalytic efficiency [28]. Hence, the potential of Ni codopant alongside N dopant to enhance the photocatalytic properties of ZrO_2-TiO_2 composite must be explored.

In this study, Ni,N-codoped ZrO_2-TiO_2 composite was synthesized using the sol-gel method, which has advantages such as high homogeneity in the resulting material, high purity in the resulting compound, low temperature used, solvent resistance in the resulting composite, and good thermal stability [29]. Various amounts of Ni dopant (2–10%) and a fixed amount of N (10%) were applied to study the codoping effect of Ni and N in ZrO_2-TiO_2 composite as photocatalysts. Various calcination temperatures (500, 700, and 900 °C) were also applied to investigate the composite properties and their effect on the photocatalytic activity to degrade MB under visible light irradiation.

■ EXPERIMENTAL SECTION

Materials

Titanium(IV) tetraisopropoxide (TTIP) (97%) as TiO_2 precursor was obtained from Sigma-Aldrich and zirconia (ZrO_2) powder was obtained from Jiaozuo Huasu. Urea ($CO(NH_2)_2$) (Merck) and nickel sulfate hexahydrate ($NiSO_4{\cdot}6H_2O$) (99%, Merck) were both selected as the sources of dopant. Ethanol (99%, Merck) and distilled water (Jaya Sentosa) were used as solvents. MB as the dye was obtained from Thermo Fisher Scientific India.

Instrumentation

Identification of functional group in the composite was performed by using Fourier transform infrared (FTIR) spectrometer Thermo Nicolet iS10. The crystal structure in the composite was studied using PANalytical X'Pert PRO MRD X-ray diffractogram (XRD, Liaoning, China Cu Kα radiation $\lambda = 1.54$ Å, 40 kV, 30 mA). The particle morphology and elemental composition of the composite surface were characterized by scanning electron microscopy equipped with energy dispersive X-ray detector (SEM-EDX) JEOL-JSM 6510 LA. Band gaps were determined based on absorption spectra from specular reflectance Pharmaspec UV 1700. The remaining amount of MB solution during photodegradation was determined by measuring the absorbance at a wavelength of 664 nm using a Thermo Scientific AQ8100 UV-vis spectrometer.

Procedure

Synthesis of Ni,N-codoped ZrO_2-TiO_2

The sol-gel method was used to prepare a Ni,N-codoped ZrO_2-TiO_2 composite [26]. Firstly, in 25.0 mL of ethanol, 2.5 mL of TTIP was added. Then, 1.00 g of ZrO_2, 86.61 mg of urea (w_N/w_{Ti} = 10%) and various amounts of $NiSO_4 \cdot 6H_2O$ (36.17, 72.33, 108.5, 144.66, and 180.83 mg) were suspended into 25 mL of distilled water. The Ni concentration was varied by weight fraction of 2, 4, 6, 8, and 10% to titanium. The suspension was then dropped into the TTIP solution and stirred for 30 min. The mixture was centrifuged at 2,000 rpm for 1 h to separate the precipitate and then left out in the open for 24 h at room temperature before being dried in an oven at 80 °C for 24 h. Afterwards, the composite was calcined at 500, 700, and 900 °C for 4 h. The composite was denoted as αNi-N-ZT-β, in which α is the weight percentage of Ni to Ti, and β is the calcination temperature (°C). Additionally, TiO_2, N-doped ZrO_2-TiO_2, and undoped ZrO_2-TiO_2 as references were prepared by the same procedure and calcined at 500 °C.

Photodegradation of methylene blue

An amount of 15 mg of Ni,N-codoped ZrO_2-TiO_2 were dispersed into 30 mL of 4 mg L^{-1} MB solution. Furthermore, the photodegradation reaction was performed for 15, 30, 45, 60, 75, 90, 105, and 120 min with continuous stirring and irradiation with LIFE MAX 30W/765 PHILIPS LTD lamps. The mixture was then centrifuged at 3,000 rpm for 30 min to separate the solid. The absorbance at 664 nm was used to calculate the concentration of MB solution after photodegradation. A kinetic model of pseudo-first order was applied to calculate the quantitative photocatalytic decomposition of methylene blue (Eq. (1) and (2)) [30]:

$$-\frac{dC}{dt} = k_{obs} C \quad (1)$$

$$\ln C = k_{obs} t + \ln C_0 \quad (2)$$

where C denotes the MB concentration (mg L^{-1}), t is the irradiation time (min), and k_{obs} is the observed rate constant of photocatalytic decomposition (min^{-1}).

■ RESULTS AND DISCUSSION

Fig. 1 displays the XRD results of Ni,N-codoped ZrO_2-TiO_2 composites calcined at 500 °C with various Ni concentrations. As reference materials, ZrO_2, TiO_2, pristine ZrO_2-TiO_2, and N-doped ZrO_2-TiO_2 composites were presented as well. According to the diffraction data, pure TiO_2 has major peaks at the 2θ regions of 25° (d_{101}) and 54° (d_{105}), which correspond to the anatase phase (01-071-1167). On the other hand, pure ZrO_2 displays peaks at the 2θ of 30° (d_{101}) and 50° (d_{112}) regions corresponding to tetragonal phase (01-081-1545). The Debye-Scherrer equation [31] was implemented to calculate the average crystallite size of Ni,N-codoped ZrO_2-TiO_2 and the results are presented in Table 1. Diffraction peaks of anatase at 2θ = 25° (d_{101}) and tetragonal at 2θ = 30° (d_{101}) were selected to determine the average crystallite sizes.

Neither the diffraction pattern of Ni crystal nor nickel oxide was observed in the XRD pattern, indicating

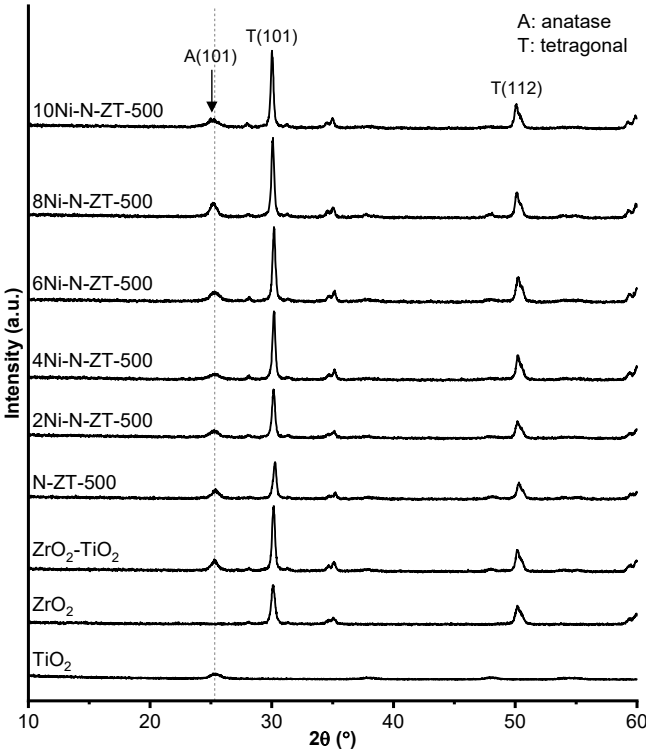

Fig 1. X-ray diffraction patterns of Ni-N-ZT-500 composites with various Ni concentrations

Table 1. Average crystallite size of Ni-N-ZT composites

Materials	Crystal phase	L (nm)
ZrO_2	Tetragonal	45
TiO_2	Anatase	20
ZrO_2-TiO_2	Anatase	59
	Tetragonal	82
N-ZT-500	Anatase	15
	Tetragonal	45
2Ni-N-ZT-500	Anatase	24
	Tetragonal	38
4Ni-N-ZT-500	Anatase	10
	Tetragonal	49
6Ni-N-ZT-500	Anatase	12
	Tetragonal	38
8Ni-N-ZT-500	Anatase	49
	Tetragonal	41
10Ni-N-ZT-500	Anatase	30
	Tetragonal	38
6Ni-N-ZT-700	Anatase	97
	Tetragonal	41
6Ni-N-ZT-900	Rutile	61
	Tetragonal	55

the inclusion of Ni^{2+} replacing Ti^{4+} in the crystal lattice [32]. The average crystallite size of the anatase phase in ZrO_2-TiO_2 is higher than TiO_2, indicating the addition of ZrO_2 promotes the crystallization of anatase. On the contrary, the addition of Ni and N dopants inhibits the crystallization of anatase, as shown by the lower average crystallite of anatase in N-ZT and all Ni-N-ZT-500 composites compared to TiO_2. The average crystallite sizes of tetragonal in all Ni-N-ZT-500 are similar compared to ZrO_2, indicating the addition of dopants gives no altercation to the tetragonal phase.

The FWHM value at the diffraction angle corresponding to the anatase phase (101) increased after Ni and N dopants were added to the optimum concentration of Ni, resulting in a decrease in ZrO_2-TiO_2 crystal size. The XRD results of 6Ni-N-ZT with various calcination temperatures are shown in Fig. 2. After calcined at 900 °C, 6Ni-N-ZT exhibits a rutile phase diffraction pattern (ICDD: 00-021-1276) at 27° (d_{110}) and 54° (d_{211}). No rutile phase was observed in 6Ni-N-ZT calcined at 500 and 700 °C, as nitrogen has been reported in the literature to inhibit the transformation from anatase to rutile [33].

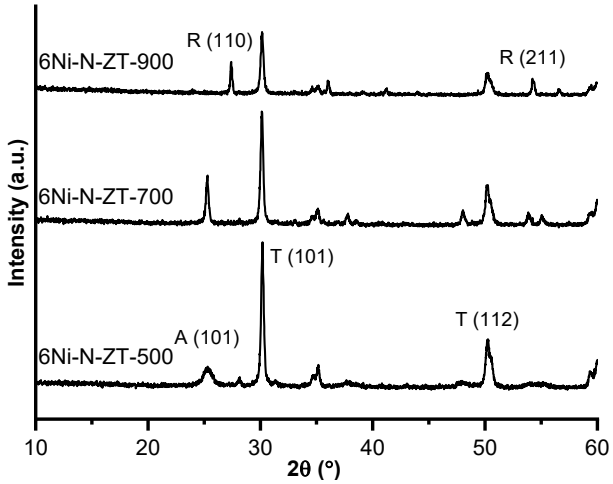

Fig 2. Diffraction patterns of 6Ni-N-ZT composites calcined at various temperatures

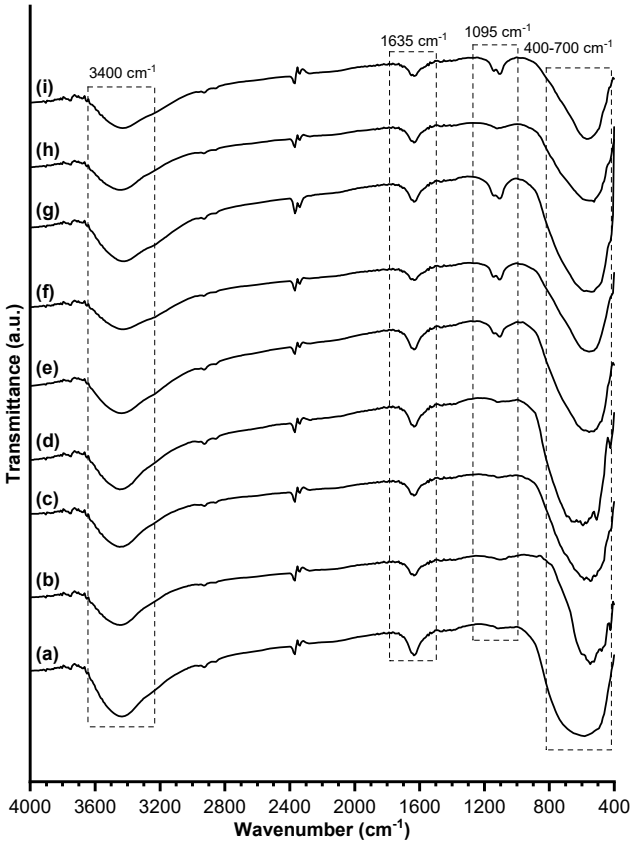

Fig 3. FTIR spectra of (a) ZrO_2, (b) TiO_2, (c) ZrO_2-TiO_2, (d) N-ZT-500, (e) 2Ni-, (f) 4Ni-, (g) 6Ni-, (h) 8Ni-, and (i) 10Ni-N-ZT-500

The FTIR spectra of Ni-N-ZT-500 with various Ni concentrations alongside ZrO_2, TiO_2, ZrO_2-TiO_2, and N-ZT-500 are shown in Fig. 3. The hydroxyl (O–H) stretching vibrations were indicated by vibrations at a wave number of around 3400 cm^{-1} that appeared in every material [34]. The bending vibration of the H–O–H group had a wavenumber of about 1635 cm^{-1} [35]. Wavenumbers less than 700 cm^{-1} exhibit overlapping absorption peaks due to stretching vibrations of Zr–O and Ti–O [36]. At a wavenumber of around 540 cm^{-1}, the stretching vibration of Zr–O with a tetragonal phase is observed [37]. The Ti–O stretching vibrations are represented by the peaks at wavenumbers 480, 500, and 570 cm^{-1} [38]. The absorption at 1095 cm^{-1} emerges as Ni dopant is introduced. It is highly possible that the absorption is the vibrational form of Ti–O–Ni due to its absence in the reference materials. Furthermore, this wavenumber is shared by the O–Zr–N and Zr–O–Ni vibrations [39].

Fig. 4 depicts the FTIR spectra of 6Ni-N-ZT at various calcination temperatures. The absorption intensity of O–H vibrations at 3400 and 1635 cm^{-1} decreases as the calcination temperature rises due to higher removal of trapped water molecules at temperatures above 500 °C. Likewise, the vibrational intensity of the Ni dopant at 1095 cm^{-1} decreases as the calcination temperature increases. This trend may be caused by high temperatures allowing Ni dopant to sinter, which reduces Ti–O–Ni vibration [40].

The band gap shown in Fig. 5(a) was determined using the SRUV spectra with the absorption edge shift method [41]. The calculated band gap of Ni-N-ZT composites is presented in Fig. 5(b). The band gaps of all Ni-N-ZT materials are lower than that of TiO_2 (3.13 eV) and N-ZT-500 (3.10 eV) [27]. This indicates that the presence of Ni and N dopants narrows the band gap and shifts the absorption edge to the visible spectrum, thus broadening the absorption spectrum. The band gap decreases from 2.91 to 2.81 eV as Ni concentration increases from 2 to 6%. With the constant nitrogen dopant concentration, the band gap increases to 2.93 eV as the Ni dopant increases to 10%. Excessive amount of Ni dopant tends to agglomerate, thus reducing the

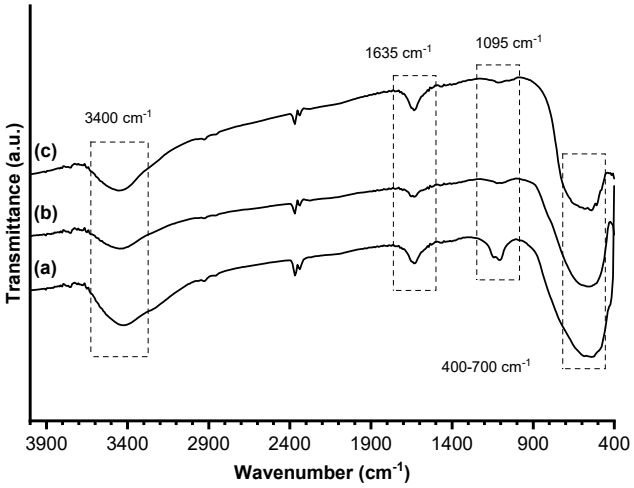

Fig 4. FTIR spectra of 6Ni-10N-ZT at (a) 500, (b) 700, and (c) 900 °C

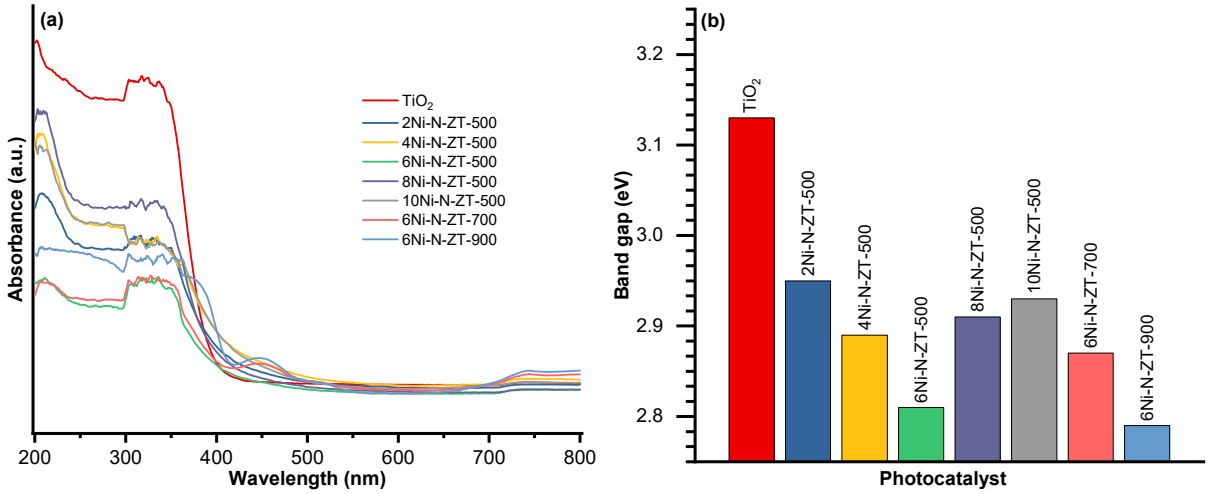

Fig 5. (a) SRUV spectra and (b) band gap of various Ni-N-ZT composites

effectiveness of doping [42]. The bandgap value of 6Ni-N-ZT decreases after calcination at 900 °C (2.79 eV). Based on the XRD data, it was clear that the anatase phase underwent a transformation to rutile, in which the band gap of the rutile phase is lower than that of the anatase phase [16]. The increasing band gap of 6Ni-N-ZT after calcination at 700 °C is due to sintering and agglomeration of Ni dopant, thus, the dopant effect decreases.

Fig. 6 displays SEM images of ZrO_2 and 6Ni-N-ZT-500 composite. ZrO_2 has uniform particle morphology, while 6Ni-N-ZT-500 composite has spherical and inhomogeneous particle morphology. Agglomeration of particles occurs because of the calcination. Table 2 shows the elemental mass percentage determined by EDX measurement of the corresponding SEM images. The presence of Ni and N dopants is confirmed on the surface of the 6Ni-N-ZT-500 composite, which are 0.24 and 1.74%, respectively. The discrepancy between expected codopants content and measured by EDX indicates the inhomogeneous distribution of Ni and N codopants on the surface of ZrO_2-TiO_2 composite. The presence of carbon in EDX results possibly comes from the carbon tape of SEM sample holder. A small number of dopants was used to prevent the formation of recombination centers and thus reduce photocatalytic activity [43]. The XRD and SRUV data show that even a small percentage of dopants influence the crystal structure and photocatalytic activity of the material.

The photocatalytic activity of Ni-N-ZT composite was evaluated by conducting photodegradation of MB in visible light using a LIFE MAX 30W/765 PHILIPS LTD lamp. Fig. 7(a) depicts the MB degradation percentage over reaction time. Photocatalytic degradation of MB proceeds as follows [27,44]:

$$\text{Photocatalyst} + hv\ (\text{photon}) \rightarrow h^+(\text{hole}) + e^-(\text{electron})$$

$$e^- + O_2 \rightarrow \bullet O^{2-}$$

$$h^+ + OH^- \rightarrow \bullet OH$$

$$\bullet O^{2-} + MB \rightarrow CO_2 + H_2O$$

$$\bullet OH + MB \rightarrow CO_2 + H_2O$$

The degradation percentage increases when exposed to visible light because photons could excite the photocatalyst, causing the generation of •OH radicals from water molecules [22]. When the photocatalyst was irradiated, hole (h^+) and electron (e^-) reacted with water and oxygen molecules, respectively, to form •OH and $\bullet O^{2-}$ radicals, which could degrade MB into carbon dioxide and water [44]. Fig. 7(b) depicts the MB degradation rate constants of various Ni-N-ZT-500 calculated from the kinetic model of pseudo-first-order [30] which are plotted against the band gap and average anatase crystallite size. Ni and N dopants can boost the photocatalytic activity of ZrO_2-TiO_2 [45]. The photocatalytic activity of the 6Ni-N-ZT-500 material is the highest, which exhibits the lowest band gap among the composite calcined at 500 °C with various Ni content. The XRD and SRUV data showed that even a small percentage of dopants influenced the crystal structure and photocatalytic activity of the material. To prevent the formation of recombination centers and thus reduce photocatalytic activity, a small number of

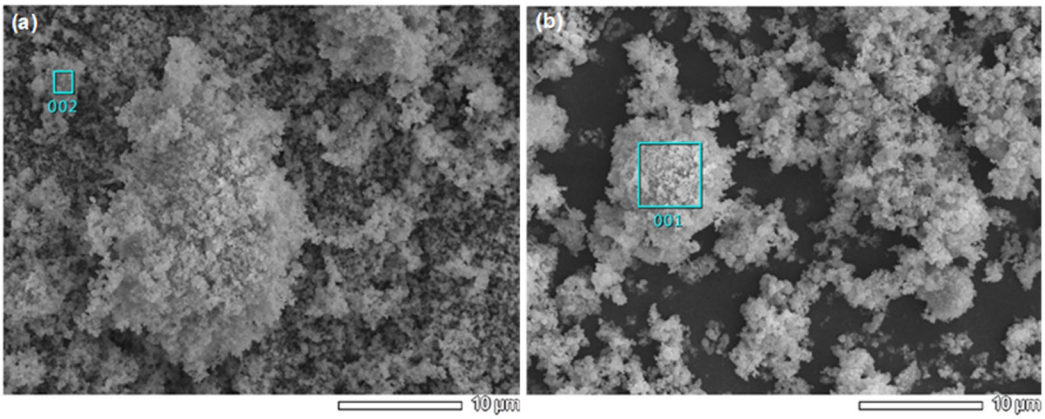

Fig 6. SEM images of (a) ZrO_2 and (b) 6Ni-N-ZT-500

Table 2. Elemental composition of ZrO_2 and 6Ni-N-ZT-500 surface measured by X-ray energy dispersive spectroscopy

Materials	% Mass						
	Zr	O	Ti	Ni	N	C	Total
ZrO_2	58.79	29.40	-	-	-	11.81	100
6Ni-10N-ZT-500	51.82	32.86	3.13	0.24	1.74	10.21	100

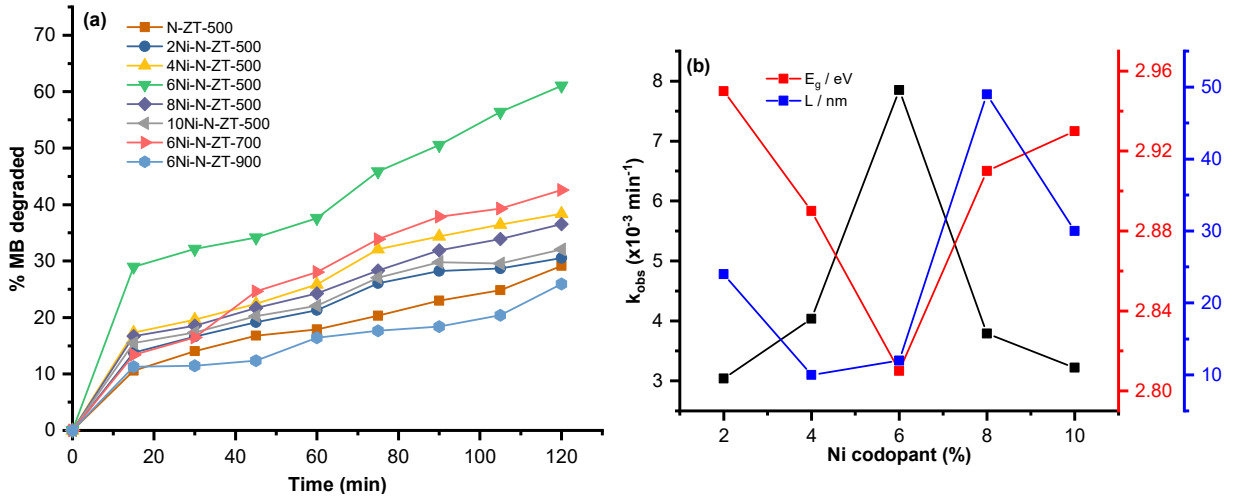

Fig 7. (a) Percentage of MB degraded for 120 min and (b) plot of observed rate constant k_{obs} of various Ni-N-ZT-500 against band gap E_g and average crystallite size of anatase L

Table 3. Comparisons of other metallic codopants in N-doped ZrO_2-TiO_2 and their properties

Metal codoping	Reaction time (min)	%MB degraded	E_g (eV)	L anatase (nm)
6% Ni	120	61	2.81	12
4% Cu [27]	120	83	2.71	34
6% Mn [46]	120	70	2.64	27

dopants was used [43]. Increasing the concentration of Ni dopant above 6% reduces photocatalytic activity, caused by Ni doping saturation, supported by the increasing band gap and average anatase crystallite size. The photocatalytic activity decreases with increasing calcination temperature, as evidenced by the material 6Ni-N-ZT-900, which has the lowest degradation percentage due to phase transformation into rutile at 900 °C. The performance of the photocatalyst is strongly influenced by the crystallinity and size of the Ni-N-ZT crystals that have been synthesized. The anatase phase demonstrates a better photocatalytic activity than the rutile phase.

In comparison to previous works [27,46], the influence of Ni codoping in N-doped ZrO_2-TiO_2 composite gives lesser activity in degrading MB compared to Cu or Mn as codopants. As shown in Table 3, the lower performance of Ni codoping effect is caused by a higher band gap, which absorbs a narrower light spectrum, and the smaller average crystallite size of anatase, which is considered the active crystallite phase [47].

■ CONCLUSION

The sol-gel method was implemented to synthesize Ni,N-codoped ZrO_2-TiO_2. Codoping of Ni and N into the ZrO_2-TiO_2 reduces the band gap and shifts the absorption edge toward visible light. FTIR analysis reveals that the vibrations of Ti–O–Ni at wavenumber 1095 cm^{-1} intensify until 6% Ni dopant addition. The ZrO_2 coupling suppresses the anatase to rutile transformation at calcination temperatures above 500 °C. Ni,N-codoped ZrO_2-TiO_2 is photo-responsive to visible light and able to degrade 4 mg L^{-1} MB solution up to 61% after

120 min of irradiation time. It has also been showed that materials have the potential to decompose dyes when exposed to visible light. Additional research on photocatalyst applications other than photodegradation and reusability test is required.

■ ACKNOWLEDGMENTS

The first author is grateful for 70/UN1/FMIPA.1.3/KP/PT.01.03/2023 Grant from The Faculty of Mathematics and Natural Sciences Universitas Gadjah Mada.

■ CONFLICT OF INTEREST

All authors certify that they have no affiliations with or involvement in any organization or entity with any financial interest or non-financial interest in the subject matter or materials discussed in this manuscript.

■ AUTHOR CONTRIBUTIONS

Akhmad Syoufian served as research supervisor, checked revision results, provided suggestion for improvements, conducted final assessments of the data and the written report. Rian Kurniawan checked revision results, and provided suggestion for improvements written report.

■ REFERENCES

[1] Thabede, P.M., Shooto, N.D., and Naidoo, E.B., 2020, Removal of methylene blue dye and lead ions from aqueous solution using activated carbon from black cumin seeds, *S. Afr. J. Chem. Eng.*, 33, 39–50.

[2] Abu-Nada, A., Abdala, A., and McKay, G., 2021, Removal of phenols and dyes from aqueous solutions using graphene and graphene composite adsorption: A review, *J. Environ. Chem. Eng.*, 9 (5), 105858.

[3] Akpomie, K.G., and Conradie, J., 2020, Advances in application of cotton-based adsorbents for heavy metals trapping, surface modifications and future perspectives, *Ecotoxicol. Environ. Saf.*, 201, 110825.

[4] Bayramoglu, G., Kunduzcu, G., and Arica, M.Y., 2020, Preparation and characterization of strong cation exchange terpolymer resin as effective adsorbent for removal of disperse dyes, *Polym. Eng. Sci.*, 60 (1), 192–201.

[5] Badawi, A.K., and Zaher, K., 2021, Hybrid treatment system for real textile wastewater remediation based on coagulation/flocculation, adsorption and filtration processes: Performance and economic evaluation, *J. Water Process Eng.*, 40, 101963.

[6] Wang, X., Xia, J., Ding, S., Zhang, S., Li, M., Shang, Z., Lu, J., and Ding, J., 2020, Removing organic matters from reverse osmosis concentrate using advanced oxidation-biological activated carbon process combined with Fe^{3+}/humus-reducing bacteria, *Ecotoxicol. Environ. Saf.*, 203, 110945.

[7] Al-Sakkaf, M.K., Basfer, I., Iddrisu, M., Bahadi, S.A., Nasser, M.S., Abussaud, B., Drmosh, Q.A., and Onaizi, S.A., 2023, An up-to-date review on the remediation of dyes and phenolic compounds from wastewaters using enzymes immobilized on emerging and nanostructured materials: Promises and challenges, *Nanomaterials*, 13 (15), 2152.

[8] Dória, A.R., Pupo, M., de Oliveira Santiago Santos, G., da Silva Vilar, D., Torres, N.H., Romanholo Ferreira, L.F., Cavalcanti, E.B., Eguiluz, K.I.B., and Salazar-Banda, G.R., 2020, Electrochemical oxidation of indanthrene blue dye in a filter-press flow reactor and toxicity analyses with *Raphidocelis subcapitata* and *Lactuca sativa*, *Ecotoxicol. Environ. Saf.*, 198, 110659.

[9] Al-Tohamy, R., Ali, S.S., Li, F., Okasha, K.M., Mahmoud, Y.A.G., Elsamahy, T., Jiao, H., Fu, Y., and Sun, J., 2022, A critical review on the treatment of dye-containing wastewater: Ecotoxicological and health concerns of textile dyes and possible remediation approaches for environmental safety, *Ecotoxicol. Environ. Saf.*, 231, 113160.

[10] Ulfa, M., Al Afif, H., Saraswati, T.E., and Bahruji, H., 2022, Fast removal of methylene blue via adsorption-photodegradation on TiO_2/SBA-15 synthesized by slow calcination, *Materials*, 15 (16), 5471.

[11] Vasiljevic, Z.Z., Dojcinovic, M.P., Vujancevic, J.D., Jankovic-Castvan, I., Ognjanovic, M., Tadic, N.B., Stojadinovic, S., Brankovic, G.O., and Nikolic, M.V., 2020, Photocatalytic degradation of methylene blue under natural sunlight using iron titanate nanoparticles prepared by a modified sol–gel method, *R. Soc. Open Sci.*, 7 (9), 200708.

[12] Sherly, E.D., Vijaya, J.J., Selvam, N.C.S., and Kennedy, L.J., 2014, Microwave assisted combustion synthesis of coupled ZnO-ZrO_2 nanoparticles and their role in the photocatalytic degradation of 2,4-dichlorophenol, *Ceram. Int.*, 40 (4), 5681–5691.

[13] Hamad, H., Bailón-García, E., Pérez-Cadenas, A.F., Maldonado-Hódar, F.J., and Carrasco-Marín, F., 2020, ZrO_2-TiO_2/Carbon core-shell composites as highly efficient solar-driven photo-catalysts: An approach for removal of hazardous water pollutants, *J. Environ. Chem. Eng.*, 8 (5), 104350.

[14] Huang, W.C., and Ting, J.M., 2017, Novel nitrogen-doped anatase TiO_2 mesoporous bead photocatalysts for enhanced visible light response, *Ceram. Int.*, 43 (13), 9992–9997.

[15] Wang, H., Zhang, L., Chen, Z., Hu, J., Li, S., Wang, Z., Liu, J., and Wang, X., 2014, Semiconductor heterojunction photocatalysts: Design, construction, and photocatalytic performances, *Chem. Soc. Rev.*, 43 (15), 5234–5244.

[16] Zhang, J., Zhou, P., Liu, J., and Yu, J., 2014, New understanding of the difference of photocatalytic activity among anatase, rutile and brookite TiO_2, *Phys. Chem. Chem. Phys.*, 16 (38), 20382–20386.

[17] Dutta, H., Nandy, A., and Pradhan, S.K., 2016, Microstructure and optical characterizations of mechanosynthesized nanocrystalline semiconducting $ZrTiO_4$ compound, *J. Phys. Chem. Solids*, 95, 56–64.

[18] Guerrero-Araque, D., Ramírez-Ortega, D., Acevedo-Peña, P., Tzompantzi, F., Calderón, H.A., and Gómez, R., 2017, Interfacial charge-transfer process across ZrO_2-TiO_2 heterojunction and its impact on photocatalytic activity, *J. Photochem. Photobiol., A*, 335, 276–286.

[19] Zhang, J., Li, L., Xiao, Z., Liu, D., Wang, S., Zhang, J., Hao, Y., and Zhang, W., 2016, Hollow sphere TiO_2-ZrO_2 prepared by self-assembly with polystyrene colloidal template for both photocatalytic degradation and H_2 evolution from water splitting, *ACS Sustainable Chem. Eng.*, 4 (4), 2037–2046.

[20] Takahashi, H., Sunagawa, Y., Myagmarjav, S., Yamamoto, K., Sato, N., and Muramatsu, A., 2003, Reductive deposition of Ni-Zn nanoparticles selectively on TiO_2 fine particles in the liquid phase, *Mater. Trans.*, 44 (11), 2414–2416.

[21] Sun, X., Liu, H., Dong, J., Wei, J., and Zhang, Y., 2010, Preparation and characterization of Ce/N-codoped TiO_2 particles for production of H_2 by photocatalytic splitting water under visible light, *Catal. Lett.*, 135 (3), 219–225.

[22] Kim, C.S., Shin, J.W., Cho, Y.H., Jang, H.D., Byun, H.S., and Kim, T.O., 2013, Synthesis and characterization of Cu/N-doped mesoporous TiO_2 visible light photocatalysts, *Appl. Catal., A*, 455, 211–218.

[23] Samangsri, S., Areerob, T., and Chiarakorn, S., 2023, Development of visible light-responsive N-doped TiO_2/SiO_2 core–shell nanoparticles for photocatalytic degradation of methylene blue dye, *Res. Chem. Intermed.*, 49 (4), 1649–1664.

[24] Asahi, R., Morikawa, T., Irie, H., and Ohwaki, T., 2014, Nitrogen-doped titanium dioxide as visible-light-sensitive photocatalyst: Designs, developments, and prospects, *Chem. Rev.*, 114 (19), 9824–9852.

[25] Chaudhari, S.M., Gawal, P.M., Sane, P.K., Sontakke, S.M., and Nemade, P.R., 2018, Solar light-assisted photocatalytic degradation of methylene blue with Mo/TiO_2: A comparison with Cr- and Ni-doped TiO_2, *Res. Chem. Intermed.*, 44 (5), 3115–3134.

[26] Hayati, R., Kurniawan, R., Prasetyo, N., Sudiono, S., and Syoufian, A., 2022, Codoping effect of nitrogen (N) to iron (Fe) doped zirconium titanate ($ZrTiO_4$) composite toward its visible light responsiveness as photocatalysts, *Indones. J. Chem.*, 22 (3), 692–702.

[27] Rahmawati, L., Kurniawan, R., Prasetyo, N., Sudiono, S., and Syoufian, A., 2023, Copper-and-nitrogen-codoped zirconium titanate (Cu-N-$ZrTiO_4$) as a photocatalyst for photo-degradation of methylene blue under visible-light irradiation, *Indones. J. Chem.*, 23 (2), 416–424.

[28] Zhang, X., and Liu, Q., 2008, Visible-light-induced degradation of formaldehyde over titania photocatalyst co-doped with nitrogen and nickel, *Appl. Surf. Sci.*, 254 (15), 4780–4785.

[29] Adam, F., and Chua, J.H., 2004, The adsorption of palmytic acid on rice husk ash chemically modified

with Al(III) ion using the sol-gel technique, *J. Colloid Interface Sci.*, 280 (1), 55–61.

[30] Syoufian, A., and Nakashima, K., 2008, Degradation of methylene blue in aqueous dispersion of hollow titania photocatalyst: Study of reaction enhancement by various electron scavengers, *J. Colloid Interface Sci.*, 317 (2), 507–512.

[31] Cong, Y., Zhang, J., Chen, F., and Anpo, M., 2007, Synthesis and characterization of nitrogen-doped TiO_2 nanophotocatalyst with high visible light activity, *J. Phys. Chem. C*, 111 (19), 6976–6982.

[32] Wang, Q., Jin, R., Zhang, M., and Gao, S., 2017, Solvothermal preparation of Fe-doped TiO_2 nanotube arrays for enhancement in visible light induced photoelectrochemical performance, *J. Alloys Compd.*, 690, 139–144.

[33] Suwannaruang, T., Kidkhunthod, P., Chanlek, N., Soontaranon, S., and Wantala, K., 2019, High anatase purity of nitrogen-doped TiO_2 nanorice particles for the photocatalytic treatment activity of pharmaceutical wastewater, *Appl. Surf. Sci.*, 478, 1–14.

[34] El-Sherbiny, S., Morsy, F., Samir, M., and Fouad, O.A., 2014, Synthesis, characterization and application of TiO_2 nanopowders as special paper coating pigment, *Appl. Nanosci.*, 4 (3), 305–313.

[35] León, A., Reuquen, P., Garín, C., Segura, R., Vargas, P., Zapata, P., and Orihuela, P.A., 2017, FTIR and Raman characterization of TiO_2 nanoparticles coated with polyethylene glycol as carrier for 2-methoxyestradiol, *Appl. Sci.*, 7 (1), 49.

[36] Doufar, N., Benamira, M., Lahmar, H., Trari, M., Avramova, I., and Caldes, M.T., 2020, Structural and photochemical properties of Fe-doped ZrO_2 and their application as photocatalysts with TiO_2 for chromate reduction, *J. Photochem. Photobiol., A*, 386, 112105.

[37] Reddy, C.V., Reddy, I.N., Reddy, K.R., Jaesool, S., and Yoo, K., 2019, Template-free synthesis of tetragonal Co-doped ZrO_2 nanoparticles for applications in electrochemical energy storage and water treatment, *Electrochim. Acta*, 317, 416–426.

[38] Alijani, M., Kaleji, B.K., and Rezaee, S., 2017, Improved visible light photocatalytic activity of TiO_2 nano powders with metal ions doping for glazed ceramic tiles, *Opt. Quantum Electron.*, 49 (6), 225.

[39] Agorku, E.S., Kuvarega, A.T., Mamba, B.B., Pandey, A.C., and Mishra, A.K., 2015, Enhanced visible-light photocatalytic activity of multi-elements-doped ZrO_2 for degradation of indigo carmine, *J. Rare Earths*, 33 (5), 498–506.

[40] Nolan, N.T., Synnott, D.W., Seery, M.K., Hinder, S.J., Van Wassenhoven, A., and Pillai, S.C., 2012, Effect of N-doping on the photocatalytic activity of sol-gel TiO_2, *J. Hazard. Mater.*, 211-212, 88–94.

[41] Martínez-Castañón, G.A., Sánchez-Loredo, M.G., Martínez-Mendoza, J.R., and Ruiz, F., 2005, Synthesis of CdS nanoparticles: A simple method in aqueous media, *Adv. Technol. Mater. Mater. Process.*, 7 (2), 171–174.

[42] Riaz, N., Mohamad Azmi, B.K., and Mohd Shariff, A., 2014, Iron doped TiO_2 photocatalysts for environmental applications: Fundamentals and progress, *Adv. Mater. Res.*, 925, 689–693.

[43] Jaiswal, R., Bharambe, J., Patel, N., Dashora, A., Kothari, D.C., and Miotello, A., 2015, Copper and Nitrogen co-doped TiO_2 photocatalyst with enhanced optical absorption and catalytic activity, *Appl. Catal., B*, 168-169, 333–341.

[44] Singh, H., Sunaina, S., Yadav, K.K., Bajpai, V.K., and Jha, M., 2020, Tuning the bandgap of m-ZrO_2 by incorporation of copper nanoparticles into visible region for the treatment of organic pollutants, *Mater. Res. Bull.*, 123, 110698.

[45] Piątkowska, A., Janus, M., Szymański, K., and Mozia, S., 2021, C-, N- and S-doped TiO_2 photocatalysts: A review, *Catalysts*, 11 (1), 144.

[46] Syoufian, A., and Kurniawan, R., 2023, Visible-light-induced photodegradation of methylene blue using Mn,N-codoped $ZrTiO_4$ as photocatalyst, *Indones. J. Chem.*, 23 (3), 661–670.

[47] Luttrell, T., Halpegamage, S., Tao, J., Kramer, A., Sutter, E., and Batzill, M., 2015, Why is anatase a better photocatalyst than rutile? - Model studies on epitaxial TiO_2 films, *Sci. Rep.*, 4 (1), 4043.